



ELSEVIER

Available online at [www.sciencedirect.com](http://www.sciencedirect.com)

SCIENCE @ DIRECT®

Applied Surface Science xxx (2005) xxx–xxx

applied  
surface science[www.elsevier.com/locate/apsusc](http://www.elsevier.com/locate/apsusc)

# Influence of ambient medium on femtosecond laser processing of silicon

S. Besner, J.-Y. Degorce, A.V. Kabashin, M. Meunier\*

*Laser Processing Laboratory, Department of Engineering Physics, Ecole Polytechnique de Montréal,  
Case Postale 6079, succ. Centre-ville, Montréal, Qué., Canada H3C 3A7*

## Abstract

Femtosecond laser radiation (800 nm, 250 fs, 1 mJ/pulse) has been used to treat a Si surface in different ambient environments, namely vacuum, air and water. We show that ablation threshold and crater characteristics (diameter “ $D$ ” and shape of craters) are similar for the three media at low laser fluences, suggesting an identical radiation-related mechanism of material removal. In contrast, at high fluences the characteristic dependence of the crater size  $D^2(F)$  in the semi-logarithmic scale becomes non-linear, starting from  $F = 10, 4$  and  $2 \text{ J/cm}^2$  for vacuum, air and water, respectively, while the shape of craters becomes different for these media. The non-linear phenomena are ascribed to plasma-related ablation effects. Possible mechanisms of material removal are discussed.

© 2005 Elsevier B.V. All rights reserved.

*Keywords:* Femtosecond laser ablation in liquid; Crater characteristics; Silicon

## 1. Introduction

By now, the femtosecond laser ablation has become an increasingly popular tool to modify surfaces of different materials. It is accepted that the femtosecond pulses give two major advantages to micromachining compared to nanosecond and longer pulses [1,2]: (i) the reduction of the pulse energy which is necessary to induce ablation for fixed laser wavelength and focusing conditions and (ii) a significant reduction or complete removal of heat-affected zone (HAZ) and,

as a consequence, the improvement of the contour sharpness for the laser-processed structures. The second advantage is a direct consequence of the pulse being much shorter than the heat diffusion time by phonon transport. The mentioned advantages contributed to the success of the femtosecond laser technique in the processing of various materials [3–10]. However, the obtained properties of the produced structures on the target surface do not always follow anticipations of the thermal-free ablation process. In particular, it was shown that performing femtosecond laser ablation experiments in air [11] or in gases at reduced pressures results in structures with evident thermal melting phenomena, which were attributed to

\* Corresponding author. Tel.: +1 514 340 4711/4971.

*E-mail address:* [michel.meunier@polymtl.ca](mailto:michel.meunier@polymtl.ca) (M. Meunier).

the contribution of plasma-related effects. Similar melting character of crater walls was recently observed in gold ablated in liquids by a femtosecond laser at relatively high laser fluences [12]. These data show the importance of ambient medium parameters on the quality of laser processing. However, a systematic study of medium-related effects has not yet been performed.

In this paper, we compare parameters of femtosecond laser ablation of silicon in vacuum, air and water ambient media and examine properties of the processed surfaces.

## 2. Experimental setup

The femtosecond laser radiation from an amplified Ti:sapphire laser system (800 nm wavelength, 250 fs pulse duration and 1 kHz repetition rate) was used to ablate a fresh silicon(1 0 0) wafer. The experiments were carried out in air, water and vacuum ( $6.3 \times 10^{-3}$  mbar). For water tests, the wafer was placed on the bottom of a 10 mL water cuvette, filled with distilled water to a thickness of 10 mm above the target surface. The beam was focused by a Mitutoyo NIR 5 $\times$  objective with the focal length of 4 cm and the laser fluence was controlled by changing the radiation energy with the help of two attenuation “roulettes” (fine and coarse).

To control the process, the chamber with the sample was mounted on a  $x$ – $y$ – $z$  translation stage with submicron precision of the target positioning (detailed description of the laser microfabrication system is given in Ref. [13]). The surface morphology was examined by optical microscopy (OM) and scanning electron microscopy (SEM; model Phillips XL20).

To correctly estimate absolute values of the laser fluence in our conditions (beam diameter 2.1 cm, focal distance of the objective 4 cm), we measured the beam waist (diameter of the spot corresponding to  $1/e^2$  decrease of the radiation intensity) in the focal plane of the focusing objective. For this purpose, we used a so-called “knife edge” technique, in which a Si blade-based knife was progressively moved over the focal plane of the laser beam, blocking some of its radiation power, while the power of the passed beam was recorded behind the focal plane by a photodetector (Ohir Nova power meter, Ophir PD-300 photodiode).

The obtained value of the waist, averaged over four different knife paths, was  $4.1 \pm 0.2 \mu\text{m}$  at  $1/e^2$ . Note that in our previous paper [12], the waist was estimated using appropriate software, simulating parameters of the focused beam for concrete parameters of the system objective. This theoretical estimation was, of course, less precise, providing slightly lower values of the waist and, as a consequence, elevated absolute values of laser fluences. Actual fluences on the target surface vary from  $60 \text{ J/cm}^2$  to  $300 \text{ J/cm}^2$ .

## 3. Results and discussion

For a correct comparison of ablation parameters for three different ambient media, we determined the precise location of the focal plane for every medium. The focusing objective was displaced over the optical axis of the system ( $z$ -axis), while produced craters on Si were examined by SEM. All tests were done at relatively low laser energies ( $0.25 \mu\text{J}$ ) near the ablation threshold to avoid breakdown [11] and filamentation [14] phenomena, which could affect the crater profiles. The point corresponding to the focal plane was determined by finding the lens position providing the smallest diameter of formed craters on Si. It was found that the focal plane is much farther for water when compared to vacuum and air. This phenomenon was apparently related to the shift of the focal point toward the region behind the target due to the refraction of the radiation by water ( $n_{\text{water}} = 1.33$  compared to  $n = 1$  for vacuum and air). The point  $z = 0$  will be referred as the focal plane for both vacuum (air) and water, although the absolute focal point values are different for these media.

To determine ablation characteristics, we studied the dependence of the crater size (squared diameter,  $D^2$ ) as a function of the radiation fluence,  $F$ , which was controlled by changing the laser energy, while the target was placed in the focal point of the focusing objective. The ablation threshold was determined by a linear extrapolation of the dependence of  $D^2(F)$  in the semi-logarithmic scale, as it was done in previous studies (see, e.g., Ref. [2]). The ablation threshold was found to depend on the number of pulses used for the ablation, while the thresholds were similar for the three tested media. For 10 pulses ( $N = 10$ ), the values of the threshold fluence were  $F_{\text{vacuum}} = 0.2 \pm 0.07 \text{ J/cm}^2$ ,

$F_{\text{air}} = 0.26 \pm 0.05 \text{ J/cm}^2$  and  $F_{\text{water}} = 0.2 \pm 0.03 \text{ J/cm}^2$  for vacuum, air and water, respectively, whereas the relevant values for the single pulse regimes were slightly higher:  $F_{\text{vacuum}} = 0.38 \pm 0.09 \text{ J/cm}^2$ ,  $F_{\text{air}} = 0.41 \pm 0.04 \text{ J/cm}^2$  (the determination of the ablation threshold for water was difficult in the single pulse regime). Examples of the extrapolations of the dependence of  $D^2(F)$  for 1 and 10 pulses are shown in Figs. 1 and 2, respectively. It should be noted that the obtained values of the ablation thresholds satisfactorily agree with previous similar studies on silicon [15,16].

One can see from the dependencies  $D^2(F)$  that the linear regime was valid only for relatively low laser fluences, near the ablation threshold, up to 10, 4 and 2  $\text{J/cm}^2$  for vacuum, air and water, respectively, independently of the number of pulses used. This

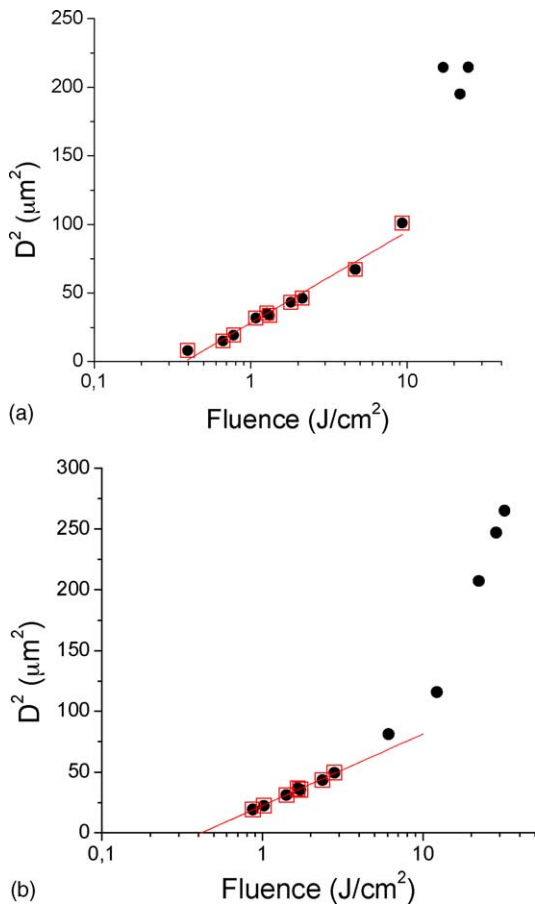


Fig. 1. Squared diameter of craters on silicon as a function of the laser fluence in the single pulse regime: (a) in vacuum; (b) in air.

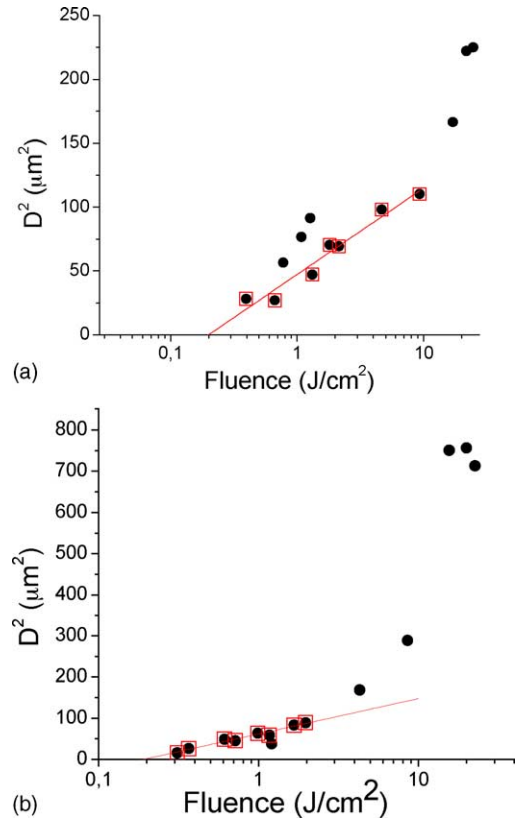


Fig. 2. Squared diameter of craters on silicon as a function of the laser fluence in the multi pulse regime ( $N = 10$ ): (a) in vacuum; (b) in water.

linear regime is consistent with conventional radiation-related ablation of material [1]. However, at higher fluences, the dependence  $D^2(F)$  became essentially non-linear, suggesting that additional ablation mechanisms are involved.

To understand the properties and mechanisms of the femtosecond ablation, we examined the target surface after laser processing. Fig. 3 shows typical SEM images of craters on Si after the femtosecond laser ablation at relatively low fluences (linear regime). As shown in the figure, both diameter and shape of the craters were almost identical for vacuum, air and water, suggesting that in this case, the medium does not affect the ablation process at low fluences. Note that craters formed in water under the multi-pulse regime do not completely overlap each other because of casual fluctuations of the water surface, affecting the focus position of the beam. In contrast, at

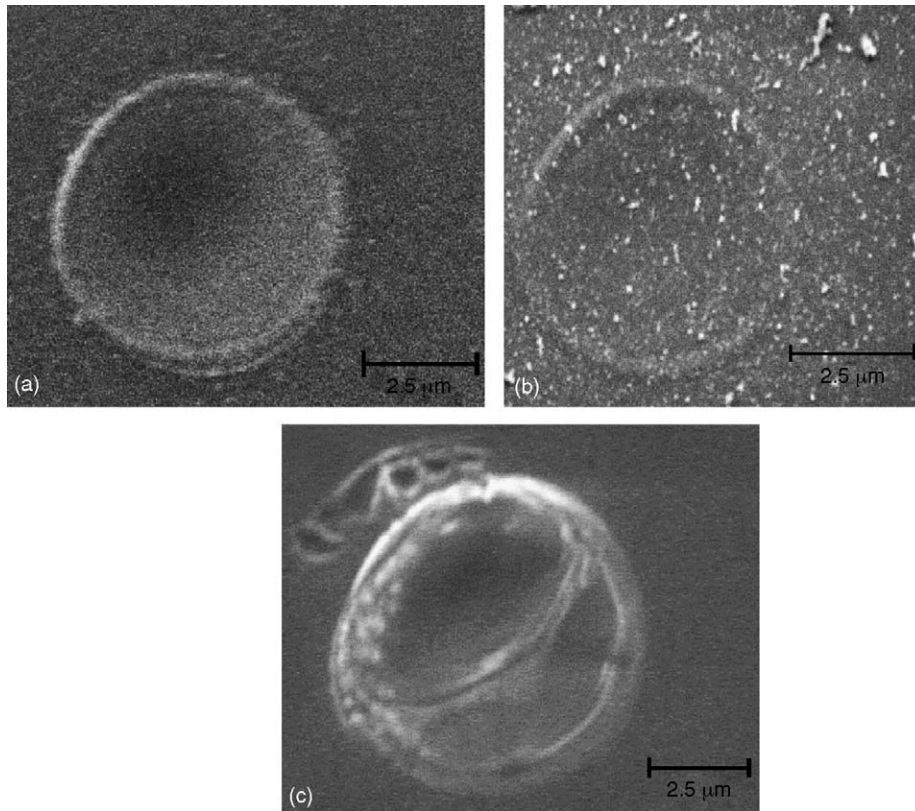


Fig. 3. Typical craters on silicon after the femtosecond laser ablation at low fluences ( $F \sim 1 \text{ J/cm}^2$ ): (a) in vacuum,  $N = 1$ ; (b) in air,  $N = 1$ ; (c) in water,  $N = 4$ .

relatively high fluences, the craters were quite different, as presented in Fig. 4. The ablation in vacuum and air at high fluences was characterized by the appearance of splash-like structures with micro-scale droplets, which were especially remarkable in the case of the laser processing in air (Fig. 4b). In addition, the femtosecond laser ablation in water led to the explosion-like removal of material with the presence of high aspect ratio columns, ripples and different irregular structures, as shown in Fig. 4c.

Our results unambiguously show the existence of two regimes of laser ablation: linear and non-linear for low and high fluences, respectively. As follows from the comparison of craters in Fig. 3, the linear regime is independent of ambient medium properties, suggesting that the primary ablation mechanism is a result from photon absorption into the materials. Indeed, as the incident pulse energy is absorbed by electrons through their interactions with one or more

photons, a series of complex phenomena occurs (including the energy transfer from electrons to phonons, phonon recombination, etc.) leading to the ablation of material within the timescale of few ps [1]. In the first approximation, the energy and the temperature distribution may be considered identical to the laser intensity distribution until the electronic and the lattice temperatures reach the equilibrium. At sufficiently high energy, ablation of the materials occurs and its profile will follow the intensity profile, provided the laser fluence is higher than the ablation threshold. The model therefore justifies the empirical relationship:

$$D^2 = 2\omega_0 \ln \left( \frac{F}{F_{th}} \right) \quad (1)$$

which does not consider any energy diffusion in the material and represents a linear tendency of the

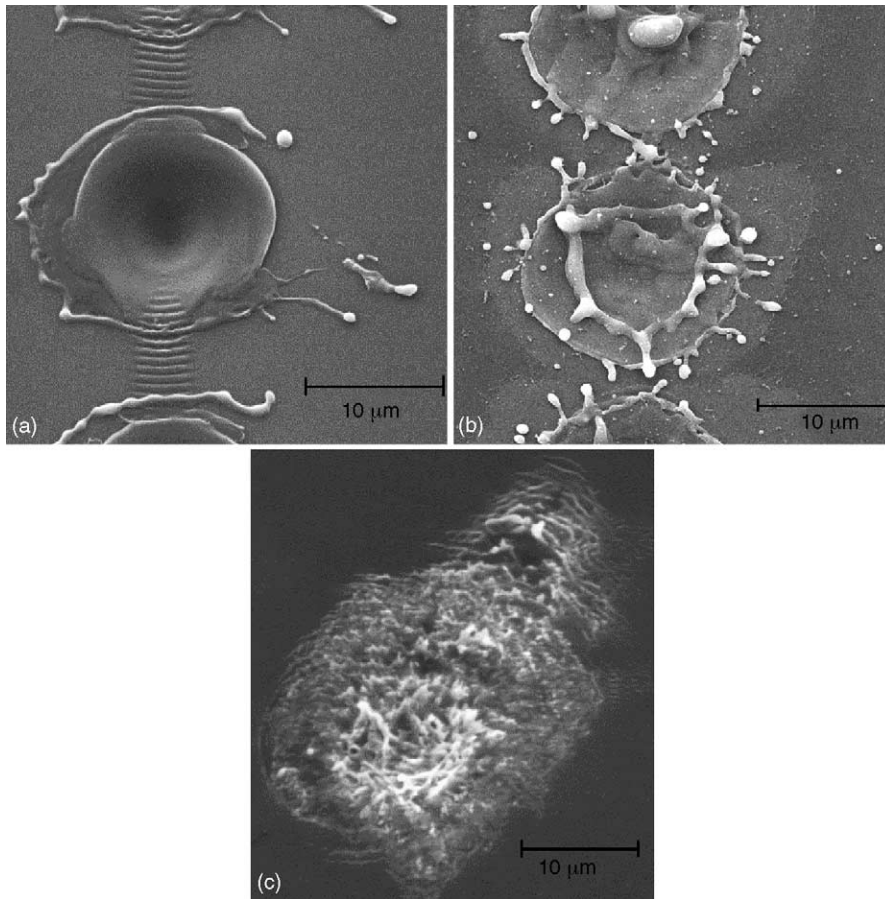


Fig. 4. Typical craters on silicon after the femtosecond laser ablation at high fluences ( $F \sim 20 \text{ J/cm}^2$ ): (a) in vacuum,  $N = 1$ ; (b) in air,  $N = 1$ ; (c) in water,  $N = 4$ .

diameter squared as a function of the fluence in the semi-logarithmic scale. Note that all obtained curves show the same threshold within the uncertainty and the same slope of  $\omega_0 = 3.8 \pm 0.4 \text{ } \mu\text{m}$ , which is in good agreement with the knife edge measurements. Therefore, we can conclude that the first linear region is primarily related to radiation-based ablation processes.

In contrast, the ablation at high fluences is characterized by a non-linear regime of the dependence  $D^2(F)$  in the semi-logarithmic scale and quite different crater shapes for vacuum, air and water environments (Fig. 4). We propose that this medium-dependent regime is due to plasma-based processes. For femtosecond pumping radiation, the ablation of material and the formation of the plasma always take place after the laser pulse. However, the formed

plasma, which might exist during several microseconds, can be hot enough to thermally melt and even evaporate the material of the target. In this case, the ablated material crystallizes upon cooling and forms splash-like microscale droplets, as it was observed in experiments performed in vacuum and especially in air (Fig. 4a and b). A quite different shape of craters formed in water (Fig. 4c) can be explained by particular properties of laser ablation in liquids. The laser–matter interaction in liquids is known to be accompanied by an energy transfer from the plasma to the nearby liquid layer, leading to the vaporization of water and, as a consequence, to the formation of bubbles [17,18]. These bubbles then quickly coalesce to form a cavitation bubble and then collapse 100–200  $\mu\text{s}$  after the laser pulse, releasing a significant amount of

mechanical energy [18]. We propose that such energy can be sufficient to cause a secondary cavitation-based ablation of material from the target surface in water yielding to an explosion-like character of craters (Fig. 4c). It should be noted that the geometric location of the plasma with respect to the target surface may also influence the plasma-based ablation process. First, the plasma can be formed by the ionized material from the target itself, which either rapidly expands in the case of vacuum or stay localized near the target surface in cases of a relatively dense air or water. Second, in air or water environment, the plasma can be formed in front of the target through the phenomenon of optical breakdown. Here, the initial absorption of radiation can take place, e.g., on easily ionized impurities in air or liquids. These phenomena could also play an important role because the fluences used are higher than the breakdown threshold, known to be around  $1 \text{ J/cm}^2$  both for water [19,20] and air [21]. To clarify the relative contributions of different plasma-based effects, one has to consider a complex model of laser–plasma–matter interactions, based on a detailed analysis of data obtained from plasma imaging and properties of the processed surfaces. These studies are in progress.

#### 4. Conclusion

In summary, we studied the influence of the ambient medium (vacuum, air and water) on properties of silicon processing by the femtosecond laser radiation. Our studies evidence the presence of different regimes of material ablation. The first one, independent of ambient medium parameters, is obtained at relatively low laser fluences and characterized by a linear dependence of squared crater diameter as the function of laser fluence ( $D^2(F)$ ) in the semi-logarithmic scale. The second one, strongly dependent on media properties, manifests itself at high fluences and is characterized by an essentially non-linear  $D^2(F)$  dependence. Radiation and plasma-related mechanisms were proposed to explain the ablation characteristics for linear and non-linear regimes, respectively.

#### Acknowledgments

We thank the Natural Sciences and Engineering Research Council of Canada for funding and J.-P. Sylvestre from École Polytechnique de Montréal for his assistance during experiments.

#### References

- [1] J.F. Ready, D.F. Farson, LIA Handbook of Laser Materials Processing, Springer-Verlag and Heidelberg GmbH & Co., Berlin, 2001.
- [2] J. Bonse, S. Baudach, J. Krüger, W. Kautek, Proc. SPIE 4065 (2000) 161.
- [3] S. Küper, M. Stuke, Appl. Phys. B 44 (1987) 199.
- [4] P. Schwab, J. Heitz, S. Proyer, D. Bäuerle, Appl. Phys. A 53 (1991) 282.
- [5] S. Preuss, E. Matthias, M. Stuke, Appl. Phys. A 59 (1994) 79.
- [6] W. Kautek, J. Krüger, Proc. SPIE 2207 (1994) 600.
- [7] J. Ihlemann, A. Scholl, H. Schmidt, B. Wolff-Rottke, Appl. Phys. A 60 (1995) 411.
- [8] J. Ihlemann, B. Wolff, P. Simon, Appl. Phys. A 54 (1992) 363.
- [9] J. Krüger, W. Kautek, Appl. Surf. Sci. 106 (1996) 383.
- [10] D. Stern, R.W. Schoenlein, C.A. Puliafto, E.T. Dobi, R. Birngruber, J.G. Fujimoto, Arch. Ophthalmol. 107 (1989) 587.
- [11] S.M. Klimentov, T.V. Kononenko, P.A. Pivovarov, S.V. Garnov, V.I. Konov, A.M. Prokhorov, D. Breittling, F. Dausinger, Quant. Electron. 31 (2001) 378.
- [12] A.V. Kabashin, M. Meunier, J. Appl. Phys. 94 (2003) 7941.
- [13] M. Meunier, B. Fiset, A. Houle, A.V. Kabashin, S.V. Broude, P. Miller, Proc. SPIE 4978 (2003) 169.
- [14] A. Brodeur, S.L. Chin, Phys. Rev. Lett. 80 (1998) 4406.
- [15] J. Bonse, S. Baudach, J. Krüger, W. Kautek, M. Lenzner, Appl. Phys. A 74 (2002) 19.
- [16] A. Cavalleri, K. Sokolowski-Tinten, J. Bialkowski, M. Schreiner, D. von der Linde, J. Appl. Phys. 85 (1999) 3301.
- [17] A. Vogel, J. Noack, K. Nahen, D. Theisen, S. Busch, U. Parltitz, D.X. Hammer, G.D. Noojin, B.A. Rockwell, R. Birngruber, Appl. Phys. B 68 (1999) 271.
- [18] P.K. Kennedy, D.X. Hammer, B.A. Rockwell, Prog. Quant. Electron. 21 (1997) 155.
- [19] D.X. Hammer, R.J. Thomas, G.D. Noojin, B.A. Rockwell, P.K. Kennedy, W.P. Roach, IEEE J. Quant. Electron. 32 (1996) 670.
- [20] J. Noack, A. Vogel, IEEE J. Quant. Electron. 35 (1999) 1156.
- [21] A. Cavalleri, K. Sokolowski-Tinten, J. Bialkowski, M. Schreiner, D. von der Linde, J. Appl. Phys. 85 (1999) 3301.